THE JOURNAL OF BIOLOGICAL CHEMISTRY
Vol. 277, No. 51, Issue of December 20, pp. 49877–49887, 2002
Printed in U.S.A.

Requirement of a Vasodilator-stimulated Phosphoprotein Family Member for Cell Adhesion, the Formation of Filopodia, and Chemotaxis in Dictyostelium*[S]

Received for publication, September 5, 2002, and in revised form, October 14, 2002
Published, JBC Papers in Press, October 17, 2002, DOI 10.1074/jbc.M209107200

Young-Hoon Han‡, Chang Y. Chung‡, Deborah Wessels§, Stephen Stephens¶, Margaret A. Titus¶, David R. Soll§, and Richard A. Firtel‡‖

From the ‡Section of Cell and Developmental Biology, Division of Biological Sciences, Center for Molecular Genetics, University of California, San Diego, La Jolla, California 92093-0634, §W. M. Keck Dynamic Image Analysis Facility, Department of Biological Sciences, University of Iowa, Iowa City, Iowa 52242, and the ¶Department of Genetics, Cell Biology, and Development, University of Minnesota, Minneapolis, Minnesota 56455

We have examined the function of a member of the vasodilator-stimulated phosphoprotein family of proteins (DdVASP) in *Dictyostelium*. *Ddvasp* null cells lack filopodia, whereas targeting DdVASP to the plasma membrane with a myristoyl tag results in a significant increase in filopodia. The proline-rich domain-Ena/VASP homology 2 structure is required for both actin polymerization activity and filopodia formation. *Ddvasp* null cells exhibit a chemotaxis defect, which appears to be due to a defect in the ability of the cells to properly adhere to the substratum and to suppress lateral pseudopod extension. We demonstrate that during chemotaxis, the anterior ~50% of the cell lifts from the substratum and remains elevated for up to 1 min. These defects lead to a significant decrease in chemotaxis efficiency. DdVASP localizes to the leading edge in migrating cells and to the tips of filopodia. In addition, *Ddvasp* null cells have a defect in particle adhesion but internalize particles normally. Our results provide new insights into the function of DdVASP in controlling the actin cytoskeleton during chemotaxis and filopodia formation.

Vasodilator-stimulated phosphoprotein (VASP)[1] was originally identified as a protein phosphorylated in response to an elevation of intracellular cAMP or cGMP levels by cAMP- and cGMP-dependent protein kinase in human platelets (1). VASP is a member of the Ena/VASP family of proteins that share a domain structure composed of three conserved domains: an N-terminal Ena/VASP homology 1 (EVH1) domain; a central proline-rich, Src homology 3-binding domain (PRD); and a C-terminal EVH2 domain. The EVH1 domain, which is also present in Wiskott-Aldrich syndrome protein (WASP) and N-WASP, binds to proteins containing the consensus sequence FPPPP, such as *Listeria monocytogenes* surface protein ActA, and interacts with the PRD of WASP (2–4). The PRD mediates VASP's interaction with the Src homology 3 domain on Src and F-actin-binding protein profilin (5–8). The EVH2 domain, which is unique to the Ena/VASP family, mediates VASP's tetramerization, F-actin binding, and actin bundling (9).

Involvement of VASP in the regulation of actin assembly and cell motility was suggested by the results of studies on actin-based movement of *Listeria*. *Listeria* movement was abolished in VASP-depleted platelet extracts and could be restored by the addition of recombinant VASP (10). VASP and EVL (Ena/VASP-like protein) induce polymerization of G-actin into F-actin bundles in *in vitro* assays in the presence of low salt and stabilize F-actin in a phosphorylation-dependent manner (10). As expected from the ability of VASP to induce actin polymerization, *in vitro* reconstitution of *Listeria* movement using purified proteins demonstrated that the speed of bacterial movement is greatly enhanced if VASP is added to the reconstitution mixture (11). These findings suggested that VASP enhances actin polymerization at a site on the *Listeria* surface to generate propelling power. The mechanism of membrane protrusion through localized actin polymerization during eukaryotic cell motility was suggested to be similar to that used in the intracellular movement of bacterial pathogens (12, 13).

The biological role of VASP in controlling cell movement and actin assembly is complex. The analysis of VASP function in axonal guidance and cell motility has produced contradictory results on the role of VASP in eukaryotic cell movement. In B16 melanoma cells, the observation that the concentration of VASP at the leading edge is directly proportional to the lamellipodial protrusion rate supports involvement of VASP in cell motility (14). Recent studies showed that VASP deficiency in murine fibroblast results in decreased cell motility in a wound healing assay due to defects in retracting the posterior of the cell and reorienting the leading edge (15). Murine Ena (Mena) is enriched in the filopodial tips of the neuronal growth cone and is required for proper axonal path-finding (16).

However, other studies support the negative role of VASP in cell motility. Overexpression of VASP in fibroblasts leads to a decrease in cell motility, whereas "depletion" of VASP from the cytosol and cortex by artificially localizing endogenous VASP to mitochondria causes an increase in cell speed (17). Similarly, Ena (*Drosophila* VASP), which binds to the cytoplasmic domain of Robo, helps mediate repulsion during axonal guidance (18). cAMP and cGMP inhibit collagen-induced platelet aggregation, which requires dynamic actin reorganization followed by cell shape change. In *vasp* null platelets, cAMP- and cGMP-

* This work was supported in part by United States Public Health Service grants (to M. A. T., D. R. S., and R. A. F.). The costs of publication of this article were defrayed in part by the payment of page charges. This article must therefore be hereby marked "*advertisement*" in accordance with 18 U.S.C. Section 1734 solely to indicate this fact.

[S] The on-line version of this article (available at http://www.jbc.org) contains two additional figures.

‖ To whom correspondence should be addressed: Center for Molecular Genetics, Room 225, University of California, San Diego, 9500 Gilman Dr., La Jolla, CA 92093-0634. Tel.: 858-534-2788; Fax: 858-822-5900; E-mail: rafirtel@ucsd.edu.

[1] The abbreviations used are: VASP, vasodilator-stimulated phosphoprotein; EVH1 and -2, Ena/VASP homology 1 and 2, respectively; PRD, proline-rich domain; WASP, Wiskott-Aldrich syndrome protein; GFP, green fluorescent protein; TRITC, tetramethylrhodamine isothiocyanate; GST, glutathione *S*-transferase.

mediated inhibition of platelet aggregation is significantly reduced (19), and *vasp* null platelets change shape very rapidly before aggregation, suggesting that VASP inhibits actin reorganization, leading to the inhibition of cell shape change and aggregation. New insight into the mechanism of VASP function in mammalian cells has been obtained through the finding that VASP controls actin filament length and its geometry under physiological (salt level) conditions by competing with F-actin capping proteins (20). Highly branched, shorter actin filaments arising from VASP deficiency are thought to be more efficient for persistent protrusion than long, unbranched filaments resulting from an excess of VASP.

To gain more insight into the role of VASP in chemotaxis, we studied the function of a *Dictyostelium* VASP family member, DdVASP, in regulating the actin cytoskeleton in unstimulated *Dictyostelium* cells and during chemotaxis by characterizing the phenotypes of *Ddvasp* null and overexpressing cells. This study further elucidates the roles of VASP in regulating the actin reorganization. We found that VASP is essential for filopodia formation, cell-substratum adhesion, and proper chemotaxis.

EXPERIMENTAL PROCEDURES

Constructs—The full sequence of the DdVASP open reading frame was amplified by PCR using a pair of primers designed from the DdVASP homologue in the *Dictyostelium* genome data base and subcloned in pBluescript KS(−). The central part of the gene from codon 111 to 228 was replaced by the blasticidin resistance cassette to make a knockout construct. For the overexpression vector, the sequences of DdVASP and constructs for various domain structures were subcloned downstream of the Actin 15 (Act15) promoter in EXP4(+). The GFP sequence was ligated in-frame to the N terminus of each DdVASP fragment to construct the GFP fusion expression vector. To target DdVASP to the membrane, the sequence for the N-terminal 16 amino acids of chicken c-Src composed of a myristoylation signal and a basic amino acid cluster sufficient for stable membrane association (21) was added in frame to the N terminus of the DdVASP sequence.

Cell Biology—Wild-type Ax3 cells were grown in HL5 medium and transformed as described previously (22). Screening for a proper knockout was performed by PCR followed by confirmation by genomic Southern blot analysis. To obtain clones overexpressing DdVASP, we selected transformants at 10 μg/ml G418 and checked the expression level of each clone by Western blot analysis.

A peptide, KGEAIRASQH, derived from the C terminus of DdVASP, was synthesized by Biosynthesis, Inc. (Lewisville, TX) for use as an antigen. Anti-DdVASP rabbit polyclonal antibody was raised against this peptide by Strategic Biosolutions (Ramona, CA). The prepared antibody was further purified by affinity chromatography as described previously (23). For indirect immunofluorescence staining, the antibody was further cleared by preabsorption of excess *Ddvasp* null cells permeabilized by treatment with 0.2% Triton X-100 for 1 min. The immunofluorescence was done as described previously (24). Analysis of subcellular localization and chemotaxis of aggregation-competent cells was performed as described by Funamoto *et al.* (22), and two-dimensional analysis was done using DIAS image analysis software (25). Cells were chosen at random with the requirement that they move for at least 10 min without touching another cell. For micropipette assays, there was no measurable difference in the average speed of the cells at the beginning or end of this period (farther away from or closer to the micropipette). Cells were examined from at least two independent experiments performed on separate days.

For three-dimensional DIAS analysis, control and *Ddvasp* null cells were grown in suspension in HL5 to a density of 2×10^6 cells/ml. To initiate development, cells were washed free of nutrient medium in basic salts solution (BSS; 20 mM KCl, 2.5 mM $MgCl_2$, and 20 mM KH_2PO_4 (pH 6.4)) and then dispersed onto filter pads as a smooth carpet at a density of 5×10^6 cells/cm^2 (26). Cells were harvested at the ripple stage of development, which represents the onset of aggregation.

For the three-dimensional analysis of cells responding to a spatial gradient of cAMP, we employed a chamber developed for the analysis of T-cell chemotaxis (27) and suitable for differential interference contrast microscopy. Cells at the ripple stage of development were allowed to adhere to a glass coverslip that was clamped over a quartz bridge (28). Video imaging and three-dimensional DIAS software analyses were done as described previously using a pixel complexity algorithm (25, 29, 30). Reconstruction of a three-dimensional faceted image of the cell surface and computation of three-dimensional parameters have been described elsewhere in detail (29). Directional change was computed as the direction in the interval $(n - 1, n)$ minus the direction in the interval $(n, n + 1)$. Height was computed as the maximum height of the faceted reconstruction. Overhang was computed as the percentage of the cell volume that does not lie directly over the portion of the cell that is attached to the substrate. The chemotactic index was determined from the three-dimensional centroid track as the net distance moved toward the source of chemoattractant divided by the total distance moved in a time period.

Quantification of F-actin levels was accomplished by measuring TRITC-phalloidin bound to F-actin as described previously (31). For the measurement of *in vitro* actin polymerization activity of DdVASP deletion mutants, GST fusion proteins were added to the *Ddvasp* null cell extract. Pulsed cells (1.5×10^8 cells) were broken in 1 ml of PMKE (12 mM sodium/potassium phosphate, pH 6.8, 2 mM $MgSO_4$, 10 mM KCl, 0.5 mM EGTA) by passage through a membrane (pore size 5 μm) and centrifuged at 10,000 $\times$ *g* for 10 min. GST fusion proteins (100 nM or 1 μM) were added immediately to the supernatant (4.3 mg/ml protein) to initiate a reaction and incubated at 22 °C. At the times indicated, 40 μl of reaction mixture was transferred to 1 ml of actin staining solution to stop the reaction. The subsequent procedure was the same as described previously (31).

Wet weight per cell was determined as follows. Vegetative cells ($\sim 10^8$ cells) grown axenically were suspended in 1 ml of HL5 containing 4 mg/ml blue dextran and pelleted by spinning at 1,500 $\times$ *g* for 2 min. The pellet was weighed and resuspended in 0.5 ml of Na/K buffer. The void volume of the pellet was calculated from the absorbance at 620 nm of the supernatant compared with the standard curve. The net weight of the pellet (total pellet weight minus the void volume of the pellet) was divided by the cell number.

Phagocytosis of fluorescent 1-μm latex beads (Polysciences, Warrington, PA) was assayed using fluorescence-activated cell sorting analysis with a modification of the original assay described by Vogel *et al.* (32), as detailed by Tuxworth *et al.* (28). The amount of latex internalized was corrected for cell size by normalizing all points to either forward scattering (which is a measure of cell size) or protein amounts using the BCA assay (Pierce). The adhesion of fluorescent 4.5-μm latex beads (Polysciences) at 0 °C was quantified as described by Tuxworth *et al.* (28). The bead binding was also normalized for cell size. A rough estimate of the cell area was obtained by measuring the two longest axes of all cells in the field and multiplying these. The phagocytosis and bead binding assays were performed in parallel with the *MVII* null mutant HTD17-1 and a control, nonhomologous transformant (28).

RESULTS

Characterization of DdVASP—The cloning of a gene encoding a *Dictyostelium* member of the Ena/VASP family of cytoskeleton regulators (DdVASP) is described under "Experimental Procedures." This is the only member of the Ena/VASP family found in the *Dictyostelium* data base. A comparison of the derived amino acid sequence of *Dictyostelium* DdVASP with VASP family members from several metazoans shows a moderately conserved primary sequence and a conserved domain structure (Fig. 1, *A* and *B*). DdVASP transcripts are expressed in vegetatively growing cells and increase upon starvation, peaking at 8 h (aggregation stage), and then remain high until fruiting body formation (Fig. 1*C*).

The gene encoding DdVASP was disrupted by homologous recombination, which was confirmed by Southern and RNA blot analyses (data not shown). Four clones were isolated. Initial experiments on these clones indicated that all exhibited similar phenotypes (data not shown). One clone was chosen for a detailed study. *Ddvasp* null cells exhibited a rate of cell division indistinguishable from that of wild-type cells. In addition, multicellular development was normal except for the formation of smaller fruiting bodies (data not shown). This is presumably due to the smaller size of the *Ddvasp* null cells, which have a cell volume that is ~60% that of wild-type cells (see "Experimental Procedures").

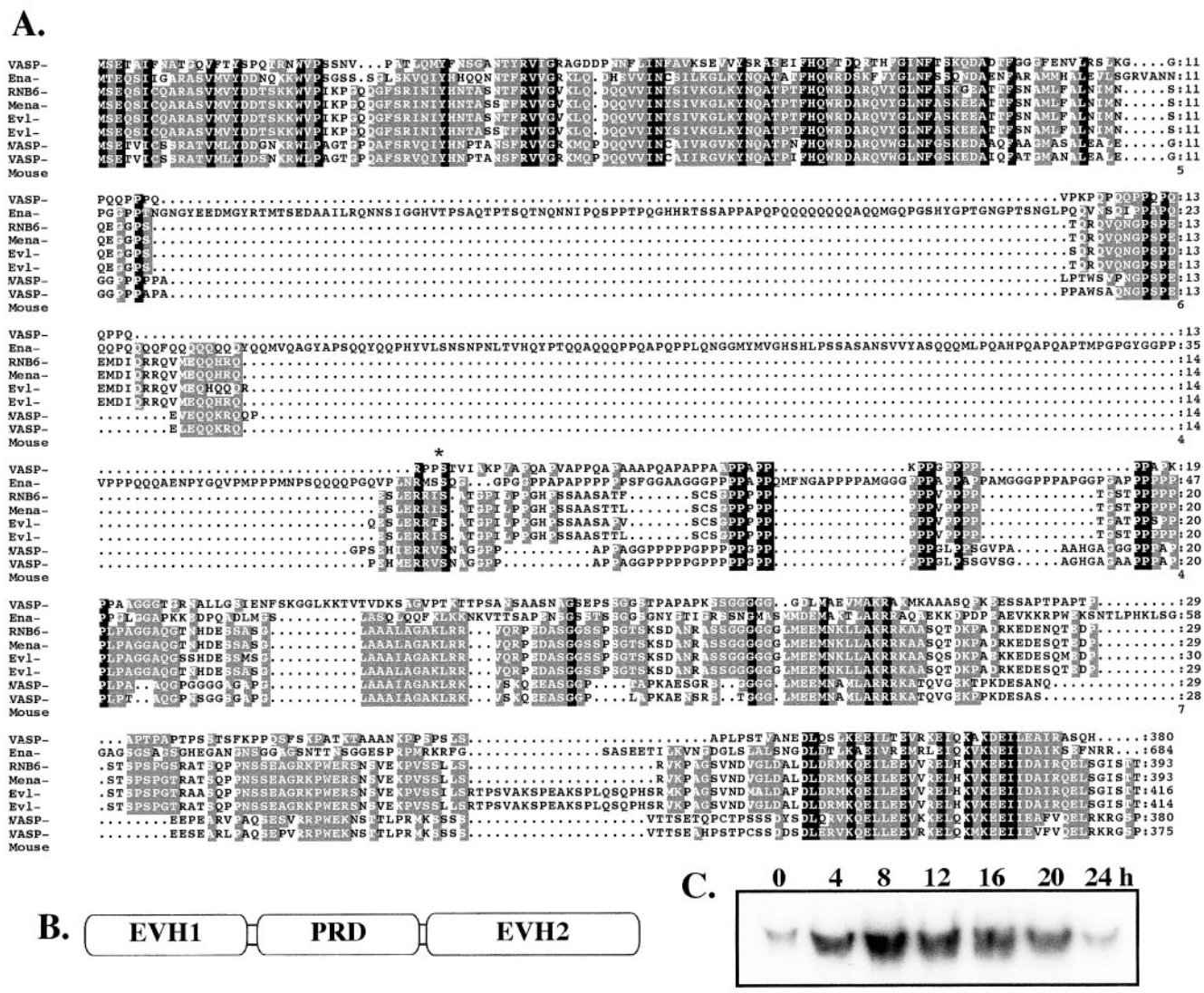

FIG. 1. **Sequence and expression kinetics of DdVASP.** *A*, comparison of the amino acid sequence of DdVASP with other VASPs (Ena (*Drosophila*), AAA85120; RNB6 (rat), JC5614; Mena (mouse), AAC52863; Evl (human), AAF17197; Evl (mouse), AAG23653; VASP (human), P50522; VASP (mouse), P70460). *B*, domain structure of DdVASP showing three distinct domains. *C*, Northern blot analysis of DdVASP expression during development. RNA was isolated from developing cells at the times indicated, and 4 μg of total RNA was loaded in each lane.

DdVASP Affects F-actin Distribution and Filopodia Formation—To examine the role of DdVASP, we created four strains that express different levels of DdVASP protein as determined by Western blot using an anti-*Dictyostelium* DdVASP antibody (Fig. 2*A*; see "Experimental Procedures"). *Ddvasp* null (*Ddvasp*$^-$) cells, as expected, have no detectable DdVASP protein (Fig. 2*A*). Strains exhibiting a level of DdVASP expression higher (DdVASP^H) or lower (DdVASP^L) than that of wild-type cells were obtained by transformation of wild-type strain KAx-3 or *Ddvasp* null cells, respectively, with a DdVASP expression vector followed by selection of clones expressing the desired level of DdVASP.

We used TRITC-phalloidin to visualize F-actin distribution in vegetative cells of the four DdVASP strains. *Ddvasp* null cells exhibit an F-actin staining pattern different from that of the other cell lines (Fig. 2*B*). In *Ddvasp* null cells, F-actin is concentrated in a few small regions around the cells' periphery. In contrast to the other DdVASP strains, the cell surfaces of *Ddvasp* null cells look smooth with no visible actin-containing, filopodia-like membrane protrusions (filopodia; Fig. 2*B*; Table I) (28), a phenotype that is strikingly similar to that of mouse embryonic stem cells lacking Cdc42, a Rho family member linked to filopodia formation (33, 34), or *Dictyostelium* cells lacking myosin VII (28). The difference in the steady-state number of filopodia and F-actin content of cell lines expressing DdVASP at various levels is summarized in Table I. Despite the observed lack of filopodia, *Ddvasp* null vegetative cells have the same F-actin level as wild-type cells. On the other hand, DdVASP^H cells are enriched in the steady-state level of filopodia on the surface and have a higher F-actin content. The lack of filopodia in *Ddvasp* null cells is rescued by expression of DdVASP, even at levels lower than expressed in wild-type cells (Fig. 2*B* and Table I, strain DdVASP^L).

Expression of Myristoylated DdVASP Leads to Increased Filopodia Formation—Since DdVASP is required for filopodia formation in *Dictyostelium*, we wanted to investigate whether membrane targeting of DdVASP would result in an elevated, steady-state level of filopodia. To pursue this question, we made use of the fact that the addition of a myristoylation tag on proteins directs them to the plasma membrane. As depicted in Fig. 2*C*, myr-DdVASP is highly enriched at the cell cortex, even in vegetative cells. As shown in Fig. 2*C* and Table I, there are large increases in F-actin content and the steady-state number of filopodia in vegetative and pulsed cells as compared with those observed in DdVASP^H cells. The average level of expression of myr-DdVASP is approximately the same as that of

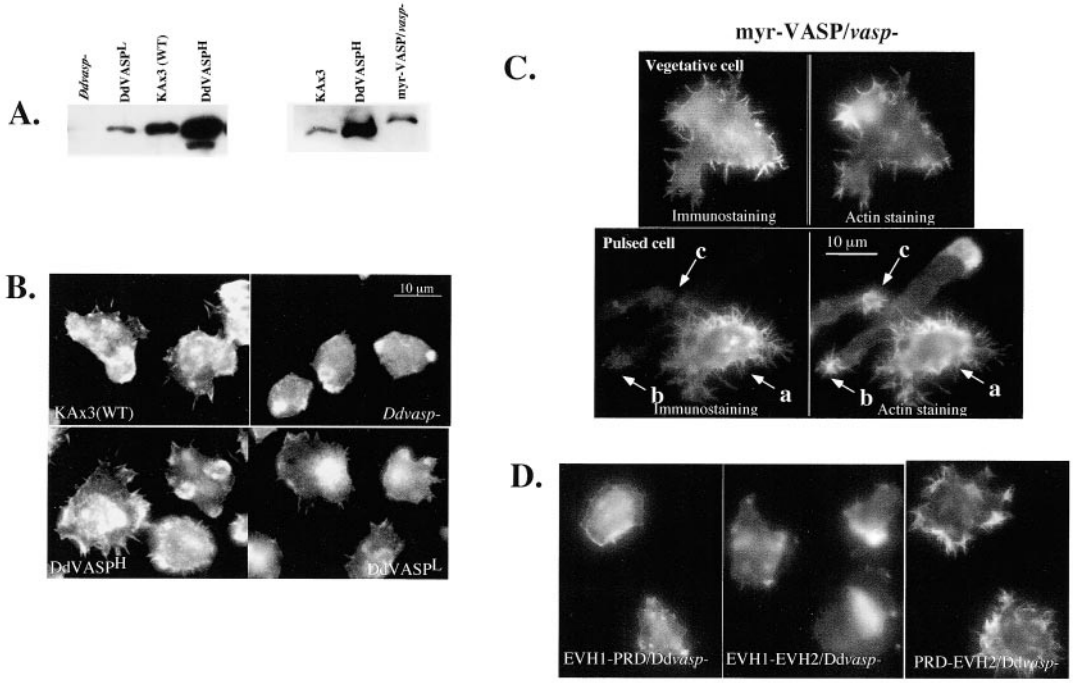

FIG. 2. **DdVASP affects F-actin distribution and filopodia formation.** *A*, DdVASP and myr-VASP expression levels. The same amount of cell extract (3 μg of total protein) from each cell line was loaded, and DdVASP was detected by immunoblot analysis using an anti-DdVASP antibody. *B*, F-actin staining with TRITC-phalloidin of vegetative cells expressing different levels of DdVASP. Cells were fixed, permeabilized, and stained. *C*, targeting of DdVASP to the cell membrane by tagging with a myristoylation sequence leads to the inhibition of cell polarization after pulsing and extensive filopodia formation. *Ddvasp* null cells expressing myr-DdVASP were immunostained with anti-DdVASP antibody and TRITC-phalloidin. *D*, F-actin staining of *Ddvasp* null cells expressing DdVASP deletion mutants. DdVASP constructs were as follows: wild-type DdVASP, residues 1–380; EVH1-PRD, residues 1–228; EVH1-EVH2, deletion of residues 111–230; PRD-EVH2, residues 111–380.

TABLE I
Correlation of steady-state filopodia number and F-actin content in VASP mutants

	Filopodia number per cell[a]	Relative F-actin level[b]	Approximate relative expression level[c]
		%	%
KAx-3 (wild type I)	7.1 ± 4.1	100	100
Ddvasp$^-$	0.9 ± 1.4	98 ± 4	0
DdVASPH	15 ± 4.8	145 ± 8	400
DdVASPL	4.6 ± 3.5	99 ± 5	50
myr-VASP/*vasp*$^-$	47 ± 18	168 ± 12	120
EVH1-PRD/*vasp*$^-$	1.1 ± 1.2	102 ± 6	300[d]
EVH1-EVH2/vasp$^-$	1.7 ± 1.3	132 ± 11	500
PRD-EVH2/*vasp*$^-$	29 ± 11	170 ± 17	350

[a] The steady-state number of filopodia in the plane of focus were counted after actin staining. 40–60 cells were counted from each cell line.
[b] F-actin contents per cell protein of vegetative cell were compared to KAx-3.
[c] Expression levels were compared by Western blot analysis using anti-DdVASP (EVH2) antibody except for EVH1-PRD/vasp$^-$.
[d] This was measured indirectly because this construct does not have the EVH2 epitope. GFP-EVH1-PRD expression level was compared with GFP-VASP expression level using anti-GFP antibody, which was in turn compared with KAx-3 using anti-DdVASP (EVH2) antibody.

endogenous DdVASP and significantly less than observed in DdVASP^H cells (Fig. 2*A*). Cells expressing higher levels of myr-DdVASP (as determined by immunostaining with the anti-DdVASP antibody) do not become polarized and have enriched F-actin in filopodia localized around the cell (Fig. 2*C*, *cell a*). Even cells expressing much lower levels of myr-DdVASP (as determined by weak immunostaining), which become polarized and are F-actin-enriched in their poles, have filopodia-like spikes protruding from one of the poles (Fig. 2*C*, *cells b* and *c*). Since these structures are not observed in wild-type cells, we conclude they result from myr-DdVASP expression. The results are consistent with membrane-targeted DdVASP being able to directly regulate the steady-state level of filopodia and possibly control filopodia formation as well as being required for their natural formation in wild-type cells.

VASP Domains Required for Filopodia Formation and Actin Polymerization—To examine which of the DdVASP subdomains is responsible for filopodia formation, we expressed various DdVASP deletion mutants, EVH1-PRD, EVH1-EVH2, and PRD-EVH2, in *Ddvasp* null cells. All proteins are expressed stably and at levels comparable with that of DdVASP in DdVASP^H cells. Previous studies indicated that recombinant human VASP is able to stimulate F-actin polymerization under low salt conditions and F-actin bundling in a cell-free system, whereas EVH2 has a weak F-actin polymerization activity but no bundling activity (10). We determined *in vitro* actin polymerization activity of subdomains as GST fusion proteins under low salt conditions and basal F-actin level of the *Ddvasp* null cell lines expressing DdVASP subdomains and compared these with the *in vivo* phenotypes of these strains. *Ddvasp* null cells expressing PRD-EVH2 resulted in even larger numbers of filopodia and a higher F-actin level than observed in DdVASP^H, whereas overexpression of EVH1-PRD or EVH1-EVH2 did not result in a significant change in filopodia number (Fig. 2*D*; Table I). PRD-EVH2 exhibited an efficacy in the *in vitro* actin polymerization assay similar to that of full-length DdVASP

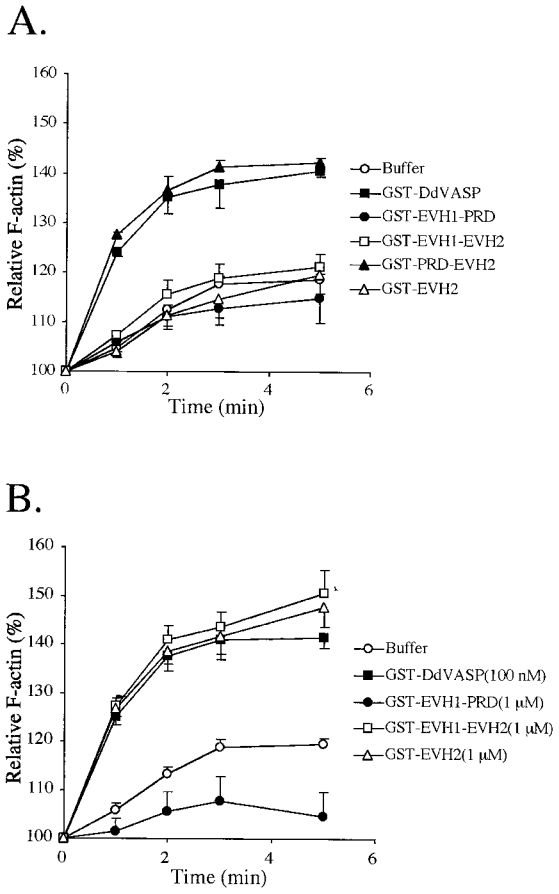

FIG. 3. **F-actin assembly activity of VASP resides in the PRD-EVH2 domain structure and EVH2 is essential for this activity.** *A*, comparison of the activity of GST fusions of subdomains to induce F-actin assembly. The same concentration (100 nM) of GST fusion proteins was added to the cell extract to initiate actin polymerization. At the times indicated, samples were taken to quantify polymerized F-actin. The amount of F-actin at the zero time point was taken as 100%. Data were collected from three separate experiments. *B*, induction of F-actin assembly by the EVH2 domain at a high concentration. A 10-fold higher concentration (1 μM) of three different domain structures was used in the assay and compared with 100 nM GST-VASP. Data were collected from three separate experiments.

(Fig. 3*A*). Expression of EVH1-EVH2 in a *Ddvasp* null cell results in a 30% increase in the F-actin level; there is no increase of filopodia formation. EVH1-PRD expression does not result in a change in the F-actin level or the number of steady-state filopodia. This finding is consistent with an absence of *in vitro* actin polymerization stimulating activity of this subdomain (Fig. 3*B*). These results suggest that the ability of DdVASP and DdVASP subdomains to promote filopodia corresponds to the ability of these domains to stimulate F-actin polymerization *in vitro* (Fig. 3).

Subcellular Localization of DdVASP—To examine the dynamic localization of DdVASP in cells, we expressed GFP-tagged DdVASP, which can complement the *Ddvasp* null cell phenotypes, in wild-type cells. In cells moving up a chemoattractant gradient, the majority of GFP-DdVASP is found dispersed in the cytoplasm; however, a bright fluorescent band is seen at the site of lamellipod/pseudopod protrusion (Fig. 4*A*). DdVASP-GFP also localizes weakly to pseudopodia in randomly migrating cells (data not shown).

We examined DdVASP localization and F-actin distribution in polarized cells by carrying out double staining of fixed cells using our anti-DdVASP antibody (see "Experimental Procedures") and TRITC-phalloidin. DdVASP immunostaining in the cell's anterior overlaps the F-actin staining (Fig. 4*C*). Under these experimental conditions, DdVASP immunostaining was diffuse at the leading edge. Interestingly, in some cells (see the cell in Fig. 4*C*), we observed a thin, more intense fluorescent band corresponding to the posterior of the F-actin-enriched domain, suggesting that the concentration of DdVASP may be highest in this region. It is possible this band may correspond to the site of highest actin polymerization. In vegetative cells, DdVASP is predominantly cytosolic, although strong staining is observed in filopodia (Fig. 4*D*), which overlaps with F-actin staining. During filopodia formation, GFP-DdVASP is transiently localized in the tip of filopodia (Fig. 4*B*). GFP-DdVASP is also localized in the cell-cell contact sites of cell aggregates (Fig. 4*B*).

DdVASP Translocates to the Cell Cortex in Response to cAMP Chemoattractant Stimulation—The F-actin binding proteins coronin and ABP-120 translocate to the cell cortex, in coordination with F-actin assembly, after global stimulation by chemoattractants, which uniformly stimulates all cell surface receptors (22, 35, 36). Fig. 5*A* shows that GFP-DdVASP also translocates to the cortex of aggregation-competent cells (cells competent to respond to the chemoattractant cAMP) (37) in response to cAMP stimulation. The fluorescence intensity at the cell cortex reaches a maximum at 6 s after cAMP stimulation and decreases thereafter, reaching a basal level by 15 s, as previously shown for coronin, although the extent of DdVASP translocation appears to be significantly less than that which we observe for GFP-coronin (22, 35). The kinetics of GFP-DdVASP translocation depicted in Fig. 5*B* are very similar to those of F-actin polymerization induced by cAMP stimulation (38).

To determine which domain is required for DdVASP localization, we prepared cell lines expressing GFP fusions of various domains of DdVASP. GFP fusions containing, but not those lacking, the EVH2 domain translocate to the cell cortex like GFP-DdVASP in response to global stimulation by cAMP (Fig. 5*B*), although the extent of the cortical localization is significantly lower than that observed with full-length DdVASP. GFP-EVH1-EVH2 showed only a very weak localization. When the aggregation-competent cells were locally stimulated by placing a micropipette tip containing cAMP close to the lateral side of a cell, GFP-DdVASP rapidly translocated to the stimulated site and remained in the new leading edge (Fig. 5*C*). This translocation was also observed in the case of GFP-EVH2 but not GFP-EVH1 (data not shown).

DdVASP Plays a Role in Chemotaxis—To examine the possible role of DdVASP in cell movement, we studied the ability of DdVASP mutant strains to polarize and chemotax up a cAMP chemoattractant gradient and analyzed the results using two-dimensional DIAS software (25). Fig. 6*A* and Table II show that *Ddvasp* null cells, although well polarized, move more slowly toward a micropipette containing cAMP than do wild-type cells and exhibit more changes in direction. *Ddvasp* null cells exhibited slightly less severe chemotaxis phenotypes using the Dunn chamber, in which there is a more uniform and possibly more reproducible chemoattractant gradient; however, we observed similar changes of direction. Comparison of cell shape between each frame reveals that *Ddvasp* null cells exhibit inefficient directional cell movement (Fig. 6*B*). In contrast, wild-type cells, which move efficiently in the direction of the chemoattractant source by extending membrane protrusions (*green*) in the direction of the source and retracting the membrane (*red*) in the rear of the cell. *Ddvasp* null cells produce lateral pseudopodia significantly more often than wild-type cells and fail to maintain the directionality of movement toward a chemoattractant gradient (Tables II and III). The anterior part of a *Ddvasp* null

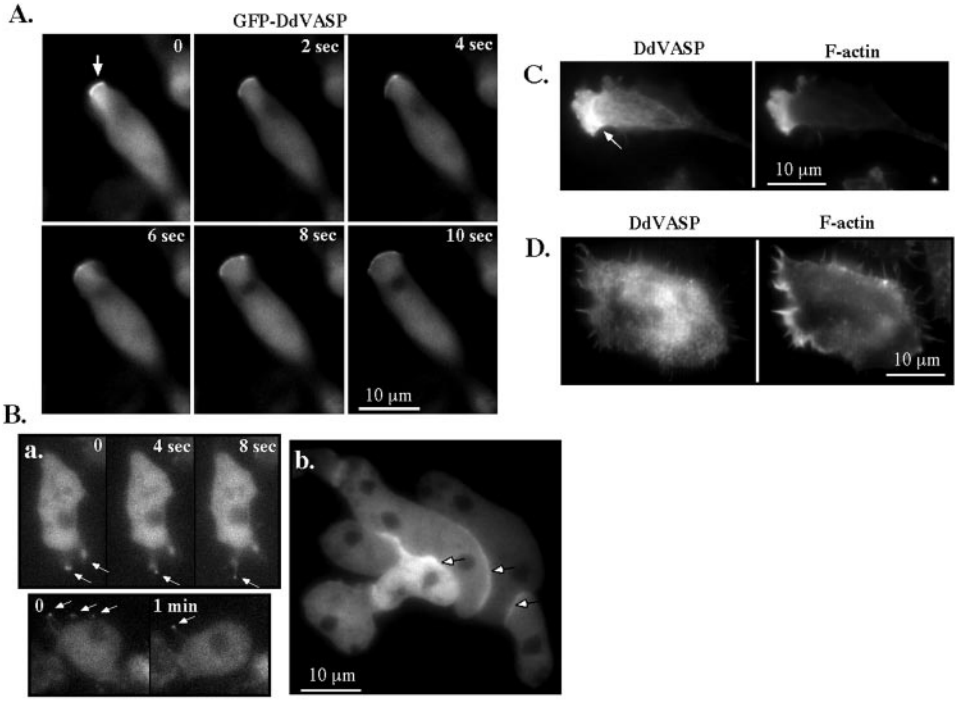

FIG. 4. **Localization of DdVASP in the leading edge and filopodia.** *A*, localization of GFP-DdVASP in the leading edge of actively moving cells. *B* (*a*), transient enrichment of GFP-DdVASP in newly forming filopodia. GFP-DdVASP overexpressing cells grown with bacteria were placed on a dish after the bacteria were washed out and recorded. The tips of filopodia enriched in GFP-DdVASP are indicated with *arrows*. *B* (*b*), localization of GFP-DdVASP in the cell-cell contact sites. An aggregate of GFP-DdVASP-expressing cells is shown. *C*, colocalization of DdVASP with F-actin in the anterior region of a DdVASP^{H} chemotaxing cell immunostained with anti-DdVASP antibody and TRITC-phalloidin. *D*, localization of DdVASP in vegetative cells in a DdVASP^{H} cell with many filopodia.

cell is lifted off the substratum in 2.2 min and does not reattach until the 4.2 min. The new leading edge then moves in a different direction than toward the chemoattractant gradient. DdVASP^{H} and DdVASP^{L} cells move slightly slower than wild-type cells, suggesting that increased or decreased DdVASP levels may lead to a reduction of directional cell movement. DdVASP^{H} cells also exhibit an increase in the number of lateral pseudopodia, indicating that increased DdVASP levels, possibly associated with the increase in F-actin, can also lead to an increase in lateral pseudopodia. Examination of stacked images of DdVASP^{H} and DdVASP^{L} chemotaxing cells reveals that DdVASP^{H} cells exhibit reduced polarity (increased roundness), whereas DdVASP^{L} cells exhibit a reduced directionality as can be seen by the increase in the number of directional changes. These differences probably account for the slight, but statistically significant, differences in the speed compared with wild-type cells. Expression of myr-VASP in *Ddvasp* null cells (myr-VASP/*Ddvasp*$^{-}$) resulted in a decrease of cell polarization (higher roundness) and more lateral pseudopodia, which in turn decrease the efficiency of chemotaxis. We observed no differences in the speed of random cell movement (movement of 1-h starved cells in buffer in the absence of a chemoattractant) between wild-type and *Ddvasp* null cells (Fig. 6*A*; Table II).

Further examination revealed that, although *Ddvasp* null cells can extend a new pseudopod, they appear defective in the adherence of the new pseudopod to the substratum. Visual analysis of the differential interference contrast movies revealed that, as the leading edge extends, it raises off the substratum and remains off the substratum for a significant period of time (data not shown). This extension of the pseudopod off the substratum is often accompanied by a change in the direction of movement. This phenotype is similar to, but possibly less severe than, that of myosin VII (*MVII*) null cells (28). Low level expression of DdVASP (DdVASP^{L} cells) in *Ddvasp* null cells complements these chemotaxis defects (data not shown).

To characterize the chemotactic defects of *Ddvasp* null cells in more detail, *Ddvasp* null cells and wild-type cells were subjected to a spatial gradient of cAMP in a quartz gradient chamber (27) in which vertical optical sections can be collected through differential interference contrast optics for dynamic three-dimensional reconstruction and motion analysis (25). In Fig. 6*C* (*a*), a representative wild-type cell moved in the direction of increasing cAMP concentration, extending a single anterior pseudopod and suppressing lateral pseudopodia over the 140 s of analysis. The anterior pseudopod lifted off the substratum periodically (Fig. 6*C* (*a*), between 40 and 65 s) and then fell back to the surface in the direction of increasing cAMP concentration, reflecting the previously described three-dimensional velocity cycle (39). This general behavior was observed in seven additional wild-type cells analyzed in the same manner (Table III). In marked contrast, the representative *Ddvasp* null mutant cell shown in Fig. 6*C* (*b*) had one pseudopod on the substratum and was in the process of forming a second pseudopod off the substratum at 0 s. As the cell retracted this pseudopod, it extended a third pseudopod that fell to the substratum at 115 s. The cell then formed new lateral pseudopodia at 130 s and turned at a right angle to the gradient at 140 s (Fig. 6*C* (*b*)). This incapacity to suppress lateral pseudopodia in a gradient was observed in five additional *Ddvasp* null mutant cells analyzed in a similar fashion and probably leads to the observed significant decrease in the chemotaxis index. *Ddvasp* null cells, therefore, were less capable of suppressing lateral pseudopod formation and generally extended off the substratum to a significantly greater degree and remained off the substratum for a longer time than wild-type cells, resulting in a dramatic loss in chemotactic efficiency. Furthermore, when the anterior of the cell lowered onto the substratum, the middle part of the cell remained off the substratum for 30 s or more (Fig. 6*C* (*b*), 60–115 s). Wild-type, DdVASP^{L}, and DdVASP^{H} cells exhibit periodic changes in speed consistent with pseudopod extension

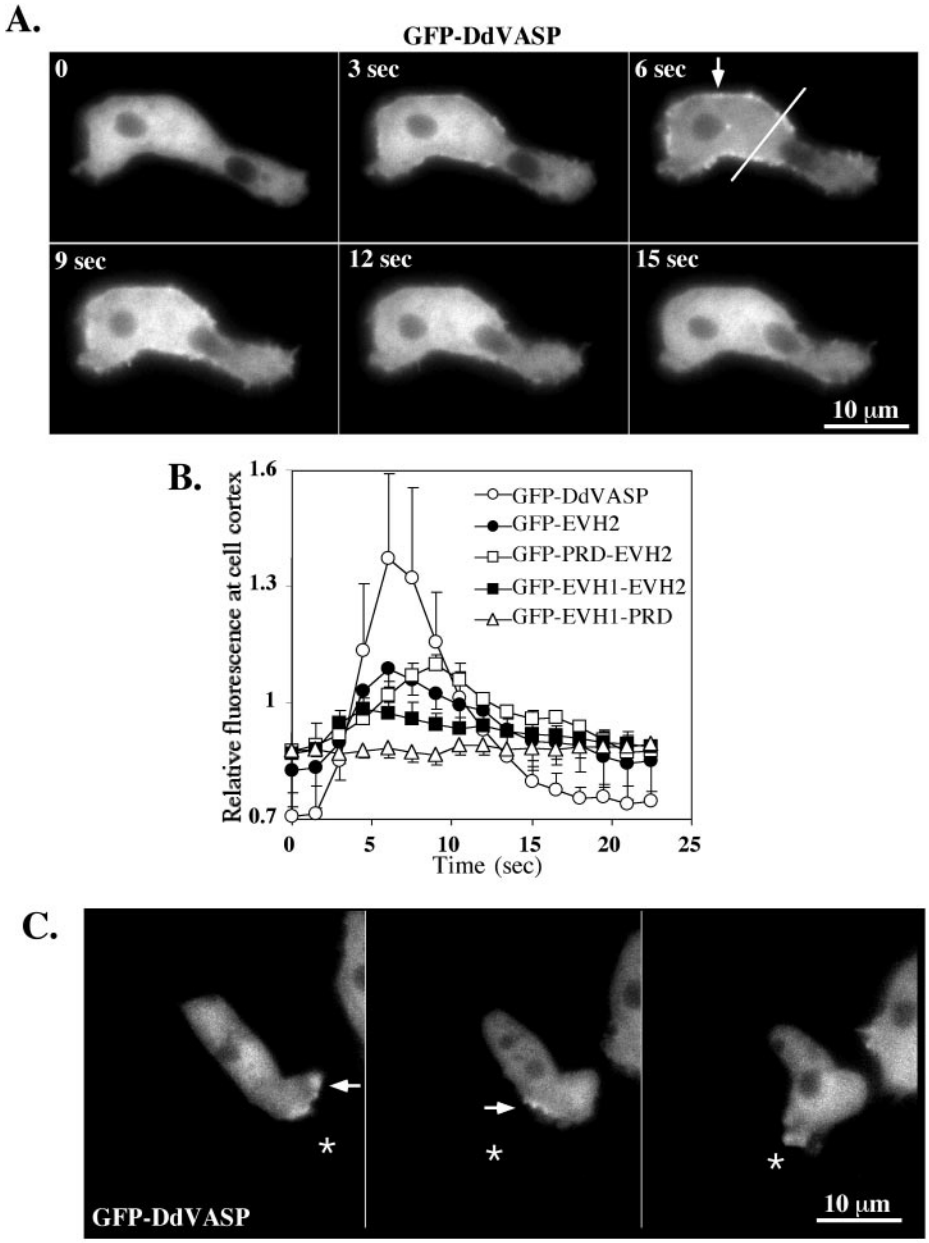

FIG. 5. **GFP-DdVASP is translocated to the cell cortex in response to cAMP stimulation in an EVH2-dependent manner.** *A*, translocation of GFP-DdVASP to the cell cortex in response to global cAMP stimulation. *B*, kinetics of translocation of GFP-DdVASP and DdVASP deletion constructs. In the case of the cell shown in *A*, the fluorescence intensity was quantitated along the line shown. The fluorescence intensity in the cell cortex was divided by that in the cytoplasm and plotted against time. Data are from at least five cells. *C*, translocation of DdVASP to the leading edge. A micropipette tip filled with 150 μM cAMP was moved to new position close to the cell, and the images were recorded. Micropipette positions are marked with *asterisks*.

followed by retraction of the uropod (data not shown). This same periodicity is lacking in *Ddvasp* null cells (Table II; data not shown).

In addition, *Ddvasp* null cells expressing myr-DdVASP or EVH1-EVH2 become multinucleate upon growth in suspension culture (see supplemental data). These cells are predominantly mononucleate when grown attached to a substratum such as a Petri dish, on which they divide by traction-mediated cytofission (40). This phenotype is similar to that of other strains, including those defective in myosin II assembly (41).

DdVASP Is Required for Particle Adhesion but Not Particle Uptake—Several aspects of the *Ddvasp* null phenotype, namely the lack of filopodia and loss of adhesion to the substrate, are strikingly similar to those recently reported for *MVII* null cells (28). As *MVII* null cells also exhibit defects in particle adhesion and uptake, we tested the ability of *Ddvasp* null cells to bind 4.5-μm latex beads at 4 °C, a measure of the presence and function of cell surface receptors. The *Ddvasp* null cells bind significantly fewer beads than control cells (1 bead per 15×10^2 μm^2 of surface area compared with 1 bead per 2.8×10^2 μm^2 of surface area) (Table IV). Although the *Ddvasp* null cells exhibit reduced particle binding, the defect is not as severe as that observed for the *MVII* null cells (1 bead bound per 42×10^2 μm^2 of surface area).

The inability to bind particles often correlates with defects in the uptake of particles in suspension. The *Ddvasp* null cells were incubated with an excess of 1-μm latex beads in suspension (150 rpm) at room temperature, and the uptake of beads over the course of 9 min was assayed by fluorescence-activated cell sorting (28). Surprisingly, after correction for the smaller size of the cells, the rate of uptake of the *Ddvasp* null cells was found to be indistinguishable from that of the control cells (data not shown). These results are in contrast to observations of *MVII* null cells assayed in parallel that exhibit a 70% decrease in uptake in comparison with the control cells.

Because of similarities between *Ddvasp* and *MVII* null cell phenotypes, we used antibodies against *Dictyostelium* MVII and *Dictyostelium* DdVASP to test for interactions between DdVASP and MVII by co-immunoprecipitation. Unstimulated or stimulated cells were lysed, and DdVASP was immunoprecipitated with anti-DdVASP antibodies and examined to determine whether MVII was co-immunoprecipitated by Western

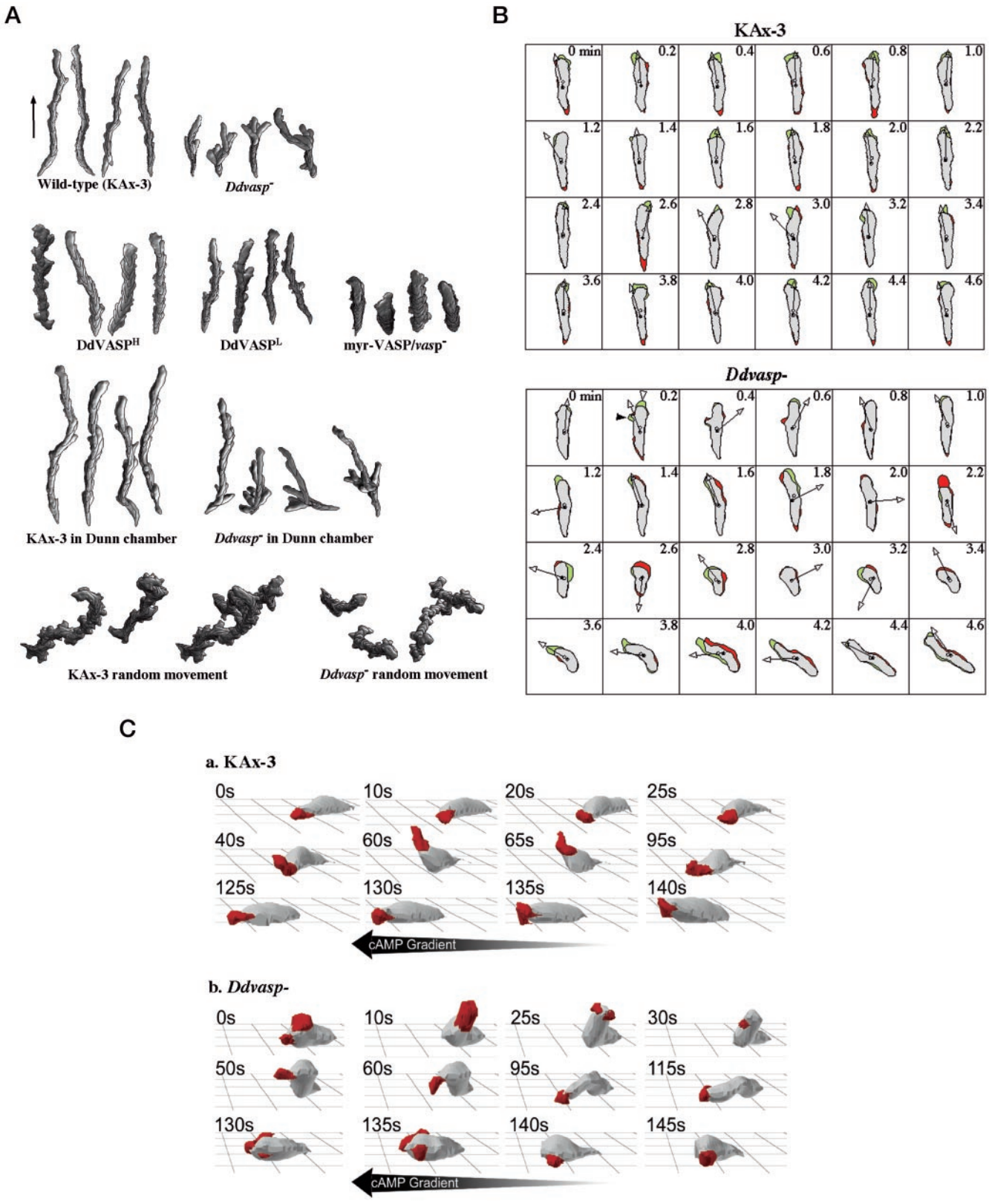

FIG. 6. **DIAS analysis of chemotaxis.** *A*, two-dimensional DIAS analysis of cell lines expressing different levels of DdVASP. Cells were traced from the movies and analyzed using DIAS software. Representatives of each cell line are shown in *stacked images*. Images taken every 1 min were superimposed. The *arrows* indicate the direction of movement. For random movement, cells were grown with bacteria and starved in sodium/potassium buffer for 1 h before recording. *B*, *Ddvasp* null cells show more frequent extrusion of lateral pseudopodia and changes in direction. Representatives of wild-type (KAx3) and *Ddvasp* null cells are shown. The shape differences between each frame (12-s interval) are shown in *green* (the newly protruded part) and *red* (the retracted part). The chemoattractant gradient is upward. The *arrows* from the centers of cells indicate the direction of movement of the centroid. Examples of anterior pseudopodia (*open arrow*) and lateral pseudopodia (*solid arrow*) are shown. *C*, three-dimensional DIAS images of representative wild-type and *Ddvasp* null cells.

TABLE II
DIAS analysis of cell movement

Strain	Speed[a]	Direction change[b]	Roundness[c]	Directionality[d]	Anterior pseudopodia	Lateral pseudopodia
	μm/min		*(%)*		*No./min*	*No./min*
Wild type (KAx-3)	9.5 ± 1.2	9.0 ± 1.1	40.3 ± 3.4	0.95 ± 0.06	1.6 ± 0.35	0.22 ± 0.096
Ddvasp$^-$	3.9 ± 1.4	35.6 ± 12.5	45.5 ± 2.8	0.44 ± 0.10	0.7 ± 0.22	0.67 ± 0.26
DdVASP^H	7.4 ± 0.5	17.2 ± 5.7	59.0 ± 2.7	0.88 ± 0.07	1.2 ± 0.43	1.04 ± 0.16
DdVASP^L	7.0 ± 0.5	17.9 ± 4.8	43.3 ± 1.8	0.83 ± 0.07	1.2 ± 0.16	0.57 ± 0.17
Myr-VASP/*vasp*$^-$	2.4 ± 0.9	36.4 ± 3.2	73.2 ± 3.7	0.63 ± 0.11	0.47 ± 0.14	0.87 ± 0.32
Wild-type (KAx-3) (Dunn chamber)	9.7 ± 0.7	6.9 ± 1.2	44.3 ± 3.4	0.96 ± 0.04	1.3 ± 0.33	0.20 ± 0.041
Ddvasp$^-$ (Dunn chamber)	6.0 ± 1.5	24.1 ± 11.4	50.3 ± 6.2	0.70 ± 0.20	0.56 ± 0.17	0.38 ± 0.12
KAx-3 (random movement)	3.7 ± 0.5	49.8 ± 5.1	60.0 ± 2.4			
Ddvasp$^-$ (random movement)	3.5 ± 0.3	49.7 ± 9.2	77.2 ± 5.1			

[a] Speed indicates speed of cell's centroid movement along the total path.
[b] Direction change is a relative measure of the number and frequency of turns the cell makes. Higher numbers indicate more turns and less efficient chemotaxis.
[c] Roundness is an indication of the polarity of the cells. Larger numbers indicate the cells are more round and less polarized.
[d] Directionality (net path length divided by total path length) is a measure of how straight the cells move. Cells moving in a straight line have a directionality of 1.0.

TABLE III
Three-dimensional-motility parameters, shape parameters, chemotactic parameters, and pseudopod dynamics in a spatial gradient of cAMP

Cell type	Cell number	Instantaneous velocity[a]	Directional change[b]	Height[c]	Overhang[d]	Chemotactic index[e]
		μm/min	*degrees/5 s*	*μm*	*%*	
KAx-3	7	13.3 ± 5.5	63 ± 20	8.8 ± 1.2	25 ± 8	+0.56 ± 0.25
Ddvasp$^-$	7	12.4 ± 5.6	65 ± 11	12.7 ± 3.5	46 ± 17	+0.11 ± 0.38
p value[f]		NS	NS	0.023	0.019	0.025

Cell type	Cell number	Anterior pseudopodia on substrate	Anterior pseudopodia off substrate	Lateral pseudopodia on substrate	Lateral pseudopodia off substrate	Frequency lateral pseudopodia
		No./min	*No./min*	*No./min*	*No./min*	*No./min*
KAx-3	8	0.40 ± 0.12	0.17 ± 0.16	0.07 ± 0.13	0.05 ± 0.09	0.11 ± 0.16
Ddvasp$^-$	6	0.18 ± 0.04	0.25 ± 0.21	0.21 ± 0.28	0.57 ± 0.27	0.78 ± 0.43
p value[f]		0.001	NS	NS	0.004	0.011

[a] Computed by drawing a line from the centroid in frame $n - 1$ to the centroid in frame $n + 1$ and then dividing the length of the line by twice the time interval between frames.
[b] The direction in the interval $(n - 1, n)$ minus the direction in the interval $(n, n + 1)$.
[c] The maximum height of the faceted reconstruction.
[d] The percentage range of the cell volume that does not lie directly over the portion of the cell that is attached to the substrate.
[e] Determined from the three-dimensional centroid track as the net distance moved towards the source of chemoattractant divided by the total distance moved in a time period.
[f] *p* values were computed by Student's *t* test. Values above 0.05 were considered nonsignificant (NS).

TABLE IV
Comparison of reduced particle-binding ability of Ddvasp null and myosin VII null cell (MVII$^-$)

Strain	*n*	Average no. of beads/cell	Mean area	Mean area per bead
			μm^2	*μm^2/bead*
KAx-3	236	0.6706	188 ± 127	2.8×10^2
MVII$^-$	259	0.0324	136 ± 91	42×10^2
Ddvasp$^-$	285	0.0751	113 ± 70	15×10^2

blot analysis. Alternatively, MVII was immunoprecipitated with anti-MVII antibodies and then examined for co-immunoprecipitation of DdVASP. No co-immunoprecipitation was observed (data not shown). We attempted to examine whether there was a genetic interaction between DdVASP and MVII by testing whether expression of myr-DdVASP in *MVII* null cells was sufficient to induce filopodia formation. We were unable to obtain stably transformed *MVII* null cells expressing high levels of myr-DdVASP, suggesting that this genetic combination is synthetically lethal, and localization of DdVASP to the plasma membrane in *MVII* null cells blocks cell growth. We obtained transient clones of *MVII* null cells expressing a lower level of myr-DdVASP. These cells did not produce filopodia (data not shown). These data suggest that MVII and DdVASP are both required for normal filopodia formation.

DISCUSSION

DdVASP Is Required for Filopodia Formation—We have combined molecular genetics with biochemical and cell biological approaches to examine the role of DdVASP in *Dictyostelium*. Analysis of vegetative *Ddvasp* null cells indicates that they are smaller than wild-type cells and lack filopodia, which are found along the periphery of wild-type cells. Membrane targeting of DdVASP using the N-terminal Src myristoylation signal results in an induction of numerous long, filopodia-like protrusions on the plasma membrane. These results strongly suggest that DdVASP is required for and can mediate filopodia formation. We observe that there is an increase in the steady-state level of filopodia in cells overexpressing wild-type or myr-VASP, suggesting that DdVASP may regulate filopodia formation in *Dictyostelium*.

Although *Ddvasp* null cells are not inherently defective in chemoattractant-mediated F-actin assembly (data not shown),

our *in vivo* and *in vitro* data indicate that DdVASP can induce actin assembly under low salt conditions, consistent with previously published studies using human VASP (10). The ability of the PRD-EVH2 construct to induce filopodia formation, as observed by an increase in the steady-state level of filopodia, correlates with the ability of DdVASP to stimulate actin assembly under our assay conditions. Recent results of Bear *et al.* (20) indicate that mammalian VASP promotes F-actin polymerization by competing with the capping protein and controls F-actin networks in the lamellipodia of moving cells. EVH2-mediated binding of VASP to the barbed end of F-actin has been suggested as the mechanism for the targeting of VASP to actin filaments and VASP's competition with capping proteins. Consistent with this suggestion, the EVH2 domain is essential for the DdVASP functions we observe. Recruitment of Cdc42 or WASP to the plasma membrane is sufficient to trigger local actin polymerization that results in filopodia formation in rat basophilic leukemia mast cells (RBL-2H3) (4, 42). It was found that VASP and zyxin, a focal adhesion protein that interacts with VASP via FPPPP motif-EVH1 interaction, are enriched in the Cdc42-induced membrane protrusions. The PRD of WASP directly interacts with the EVH1 domain of VASP, suggesting that WASP and VASP cooperate as a complex to stimulate actin assembly and membrane protrusion and thus may aid in filopodia formation. Our results indicate that in *Dictyostelium*, the EVH1 domain is not essential for the production of the membrane protrusions we observe. However, the PRD-EVH2 construct is expressed at levels that we estimate are 3–4-fold above that of the endogenous VASP protein, which may account for the differences in phenotype.

Ddvasp null cells are able to effectively sense and respond to a chemoattractant gradient but exhibit a low chemotaxis index (low persistence of movement in the direction of the chemotaxis source) due to a decrease in adhesion and a resulting increase in lateral pseudopodia formation. Both the cell adhesion defect and the lack of filopodia are phenotypes that are shared with the *Dictyostelium MVII* null cells (28). Interestingly, the *MVII* null cells are as small as the *Ddvasp* null cells, as determined by both quantification of the amount of protein per cell and forward scattering using fluorescence-activated cell sorting (data not shown), a finding which is consistent with MVII and DdVASP sharing functions. *Ddvasp* null and *MVII* null cells share a defect in particle adhesion at 0 °C, although this defect and the decrease in substratum adhesion during chemotaxis are more severe in the *MVII* null cells than in *Ddvasp* null cells. Unlike *MVII* null cells, *Ddvasp* null cells do not exhibit a defect in phagocytosis. Expression of myr-DdVASP in *MVII* null cells does not result in filopodia formation. This observation, together with all of the similarities between *Ddvasp* and *MVII* null cell phenotypes (small cell size, defects in the adherence during chemotaxis, lack of filopodia, and the defect in the particle adhesion), raise the possibility of genetic interactions between DdVASP and MVII during these processes. We were unable to detect a direct physical interaction between DdVASP and MVII.

DdVASP Is Required for Proper Chemotaxis—Our data demonstrate that *Ddvasp* null cells have a severe chemotaxis defect. The cells move very poorly and exhibit numerous changes in direction. When *Ddvasp* null cells are either elevated off or not fully adherent to the substratum, they extend multiple, lateral pseudopodia, an effect which is normally not seen in wild-type cells. As a result of the formation of the lateral pseudopodia, when the pseudopodia reassociate with the substratum, the new leading edge is often pointing in a different direction. This production of lateral pseudopodia is not as severe as that observed in *paka* null cells, which are unable to assemble myosin II in response to chemoattractant stimulation (24). Moreover, in *paka* null cells, pseudopodia extend from the lateral sides near the posterior as well as the anterior, which is not observed in *Ddvasp* null cells. During the extended period of elevation, the anterior half of the *Ddvasp* null cell often exhibits some random movement. We think these defects are the primary causes of the chemotaxis inefficiency. Overexpression or membrane targeting of DdVASP also results in chemotaxis defects. These strains exhibit an elevated F-actin content and filopodia. Furthermore, cells expressing myr-DdVASP exhibit a reduced cell polarity, possibly resulting from a uniform enrichment of DdVASP, leading to F-actin assembly along the cortex, which may also compete for the actin polymerization machinery at the leading edge.

Our results, for the first time, reveal the direct involvement of DdVASP in controlling the steady-state level of filopodia, suggesting involvement of DdVASP in filopodia formation *per se*. We also show that DdVASP is required for inhibition of pseudopod extension and adhesion of the cell to the substratum. The cell movement defects we observe in *Ddvasp* null cells were not seen in fibroblasts, possibly because of the slow rate of movement of these cells. Our analyses demonstrate that the EVH2 domain mediates DdVASP localization to the leading edge. As the EVH2 domain mediates DdVASP binding to F-actin and the localization of Ena/DdVASP to stress fibers (9), it is possible that the targeting of DdVASP to the leading edge in *Dictyostelium* cells is mediated by the interaction of the EVH2 domain with F-actin. The localization of DdVASP to the cell cortex in response to global stimulation may be similarly mediated.

Acknowledgments—We thank S. Lee (University of California, San Diego) and Jeremy Geiger (University of Iowa) for technical assistance, members of the Firtel and Titus laboratories for helpful suggestions, and J. Roth (University of California, San Diego) for critical reading of the manuscript.

REFERENCES

1. Waldmann, R., Nieberding, M., and Walter, U. (1987) *Eur. J. Biochem.* **167,** 441–448
2. Niebuhr, K., Ebel, F., Frank, R., Reinhard, M., Domann, E., Carl, U., Walter, U., Gertler, F., Wehland, J., and Chakraborty, T. (1997) *EMBO J.* **16,** 5433–5444
3. Pistor, S., Chakraborty, T., Walter, U., and Wehland, J. (1995) *Curr. Biol.* **5,** 517–525
4. Castellano, F., Le Clainche, C., Patin, D., Carlier, M. F., and Chavrier, P. (2001) *EMBO J.* **20,** 5603–5614
5. Ahern-Djamali, S., Bachmann, C., Hua, P., Reddy, S., Kastenmeier, A., Walter, U., and Hoffmann, F. (1999) *Proc. Natl. Acad. Sci. U. S. A.* **96,** 4977–4982
6. Reinhard, M., Jouvenal, K., Tripier, D., and Walter, U. (1995) *Proc. Natl. Acad. Sci. U. S. A.* **92,** 7956–7960
7. Lambrechts, A., Verschelde, J., Jonckheere, V., Goethals, M., Vandekerckhove, J., and Ampe, C. (1997) *EMBO J.* **16,** 484–494
8. Kang, F., Laine, R., Bubb, M., Southwick, F., and Purich, D. (1997) *Biochemistry* **36,** 8384–8392
9. Bachmann, C., Fischer, L., Walter, U., and Reinhard, M. (1999) *J. Biol. Chem.* **274,** 23549–23557
10. Laurent, V., Loisel, T., Harbeck, B., Wehman, A., Grobe, L., Jockusch, B., Wehland, J., Gertler, F., and Carlier, M. (1999) *J. Cell Biol.* **144,** 1245–1258
11. Loisel, T., Boujemaa, R., Pantaloni, D., and Carlier, M. (1999) *Nature* **40,** 613–616
12. Machesky, L., and Cooper, J. (1999) *Nature* **401,** 542–543
13. Machesky, L. (1999) *Nat. Cell Biol.* **1,** E29–E31
14. Rottner, K., Behrendt, B., Small, J., and Wehland, J. (1999) *Nat. Cell Biol.* **1,** 321–322
15. Garcia Arguinzonis, M. I., Galler, A. B., Walter, U., Reinhard, M., and Simm, A. (2002) *J. Biol. Chem.*, in press
16. Lanier, L., Gates, M., Witke, W., Menzies, A., Wehman, A., Macklis, J., Kwiatkowski, D., Soriano, P., and Gertler, F. (1999) *Neuron* **22,** 313–325
17. Bear, J., Loureiro, J., Libova, I., Fassler, R., Wehland, J., and Gertler, F. (2000) *Cell* **101,** 717–728
18. Bashaw, G., Kidd, T., Murray, D., Pawson, T., and Goodman, C. (2000) *Cell* **101,** 703–715
19. Aszodi, A., Pfeifer, A., Ahmad, M., Glauner, M., Zhou, X., Ny, L., Andersson, K., Kehrel, B., Offermanns, S., and Fassler, R. (1999) *EMBO J.* **18,** 37–48
20. Bear, J. E., Svitkina, T. M., Krause, M., Schafer, D. A., Loureiro, J. J., Strasser, G. A., Maly, I. V., Chaga, O. Y., Cooper, J. A., Borisy, G. G., and Gertler, F. B. (2002) *Cell* **108,** 509–521
21. Sigal, C., Zhou, W., Buser, C., McLaughlin, S., and Resh, M. (1994) *Proc. Natl.*

Acad. Sci. U. S. A. **91,** 12253–12257
22. Funamoto, S., Milan, K., Meili, R., and Firtel, R. (2001) *J. Cell Biol.* **153,** 795–810
23. Harlow, E., and Lane, D. (1988) *Antibodies: A Laboratory Manual*, Cold Spring Harbor Laboratory Press, New York, NY
24. Chung, C., and Firtel, R. (1999) *J. Cell Biol.* **147,** 559–575
25. Wessels, D., and Soll, D. (1998) in *Motion Analysis of Living Cells* (Soll, D., and Wessels, D., eds) pp. 101–140, John Wiley & Sons, Inc., New York
26. Soll, D. (1987) in *Methods in Cell Biology* (Spudich, J., ed) pp. 413–431, Academic Press, Inc., New York
27. Shutt, D., Jenkins, L., Carolan, E., Stapleton, J., Daniels, K., Kennedy, R., and Soll, D. (1998) *J. Cell Sci.* **111,** 99–109
28. Tuxworth, R., Weber, I., Wessels, D., Addicks, G., Soll, D., Gerisch, G., and Titus, M. (2001) *Curr. Biol.* **11,** 318–329
29. Soll, D., Voss, E., Johnson, O., and Wessels, D. (2000) *Scanning* **22,** 249–257
30. Soll, D., and Voss, E. (1998) in *Motion Analysis in Living Cells* (Soll, D., and Wessels, D., eds) pp. 25–52, John Wiley and Sons, Inc., New York
31. Chung, C., Lee, S., Briscoe, C., Ellsworth, C., and Firtel, R. (2000) *Proc. Natl.Acad. Sci. U. S. A.* **97,** 5225–5230
32. Vogel, G., Thilo, L., Schwarz, H., and Steinhart, R. (1980) *J. Cell Biol.* **86,** 456–465
33. Chen, F., Ma, L., Parrini, M., Mao, X., Lopez, M., Wu, C., Marks, P., Davidson, L., Kwiatkowski, D., Kirchhausen, T., Orkin, S., Rosen, F., Mayer, B., Kirschner, M., and Alt, F. (2000) *Curr. Biol.* **10,** 758–765
34. Hall, A., and Nobes, C. (2000) *Philos. Trans. R. Soc. Lond-Biol. Sci.* **355,** 965–970
35. Gerisch, G., Albrecht, R., Heizer, C., Hodgkinson, S., and Maniak, M. (1995) *Curr. Biol.* **5,** 1280–1285
36. Pang, K., Lee, E., and Knecht, D. (1998) *Curr. Biol.* **8,** 405–408
37. Insall, R., Soede, R., Schaap, P., and Devreotes, P. (1994) *Mol. Biol. Cell* **5,** 703–711
38. Hall, A., Schlein, A., and Condeelis, J. (1988) *J. Cell. Biochem.* **37,** 285–299
39. Wessels, D., Vawter-Hugart, H., Murray, J., and Soll, D. (1994) *Cell Motil. Cytoskel.* **27,** 1–12
40. Fukui, Y., De Lozanne, A., and Spudich, J. (1990) *J. Cell Biol.* **110,** 367–378
41. Firtel, R., and Chung, C. (2000) *Bioessays* **22,** 603–615
42. Castellano, F., Montcourrier, P., Guillemot, J., Gouin, E., Machesky, L., Cossart, P., and Chavrier, P. (1999) *Curr. Biol.* **9,** 351–360